

Propagation of Input Uncertainty in Presence of Model-Form Uncertainty: A Multi-fidelity Approach for CFD Applications

Jian-Xun Wang, Christopher J. Roy, Heng Xiao*

Department of Aerospace and Ocean Engineering, Virginia Tech, Blacksburg, VA 24060, United States

Abstract

Proper quantification and propagation of uncertainties in computational simulations are of critical importance. This issue is especially challenging for computational fluid dynamics (CFD) applications. A particular obstacle for uncertainty quantifications in CFD problems is the large model discrepancies associated with the CFD models used for uncertainty propagation. Neglecting or improperly representing the model discrepancies leads to inaccurate and distorted uncertainty distribution for the Quantities of Interest. High-fidelity models, being accurate yet expensive, can accommodate only a small ensemble of simulations and thus lead to large interpolation errors and/or sampling errors; low-fidelity models can propagate a large ensemble, but can introduce large modeling errors. In this work, we propose a multi-model strategy to account for the influences of model discrepancies in uncertainty propagation and to reduce their impact on the predictions. Specifically, we take advantage of CFD models of multiple fidelities to estimate the model discrepancies associated with the lower-fidelity model in the parameter space. A Gaussian process is adopted to construct the model discrepancy function, and a Bayesian approach is used to infer the discrepancies and corresponding uncertainties in the regions of the parameter space where the high-fidelity simulations are not performed. Several examples of relevance to CFD applications are performed to demonstrate the merits of the proposed strategy. Simulation results suggest that, by combining low- and high-fidelity models, the proposed approach produces better results than what either model can achieve individually.

Keywords: Uncertainty, Probability, Aerospace

1. Introduction

Computational simulations, particularly those based on numerical solutions of partial differential equations, have become an indispensable tool for decision-makers by providing predictions of system responses with quantified uncertainties. It is important yet challenging to quantify these uncertainties to provide reliable guidance for decision-making processes. When a physical system is simulated with a model, uncertainties may result from various sources, which can be broadly classified into data uncertainties and model uncertainties [1].

*Corresponding author. Tel: +1 540 231 0926
Email address: hengxiao@vt.edu (Heng Xiao)

Data uncertainties are due to intrinsic variations of the system itself or inexact characterizations thereof, including operation scenarios, initial and boundary conditions, geometry, and material properties, among others. As such, they are also known as *input uncertainties* or *parametric uncertainties*. Throughout this paper we use the flow past an airfoil as an example, which is a classical problem in Computational Fluid Dynamics (CFD). In this example, input uncertainties may originate from (1) operation conditions such as angle of attack (AoA), Reynolds number, and Mach number, (2) initial and boundary conditions of the flow field, (3) geometry of the airfoils, and (4) material properties (e.g., roughness of the airfoil surface), among others. We assume that the input uncertainties have already been adequately characterized and quantitatively represented with known probability distributions. The quantified input uncertainties are then propagated into predictions of the quantities of interest (QoIs) through the CFD models, leading to uncertainties in the output. However, the output uncertainty distribution can be distorted by the uncertainties stemmed from computational models. Model uncertainty or model discrepancy, which refers to the differences between the mathematical model and the physical reality, is a main factor affecting uncertainty propagation. Interpolation error is another factor that may affect input uncertainty propagations when the simulations are too expensive to allow for a statistically meaningful number of samples to be propagated and thus surrogate models are used. The discrepancy between the original expensive model output and the relatively cheap surrogate model output is referred to as interpolation error. There are other uncertainties associated with the numerical model, e.g., from parameter calibration and numerical discretization, which are not of particular concern here. In CFD applications, perfect models are rarely available or affordable for any nontrivial turbulent flows, and the discrepancies between model predictions and physical system responses are often appreciable. These model discrepancies distort the output uncertainties and complicate the uncertainty propagation processes. High-fidelity models of turbulent flows, being accurate (if used properly) yet expensive, can accommodate only a small ensemble of simulations and thus lead to large interpolation errors and/or sampling errors; low-fidelity models can propagate a large ensemble, but can introduce large modeling errors (e.g., when Reynolds-Averaged Navier–Stokes (RANS) model is used on flows with massive separation or strong pressure gradient). Therefore, multiple models with different fidelities are employed in this work in a complementary way to address this difficulty.

The benefits of utilizing computational models of multiple fidelities have long been recognized by the science, engineering, and statistics communities. Various statistical frameworks have been proposed to incorporate information from multiple models. Bayesian Model Averaging (BMA) method [2] and its dynamic variant [3] compute the distributions of the prediction by averaging the posterior distribution under each of the models considered, weighted by their posterior model probability. However, the fundamental assumption in BMA is that the models of concern are all plausible, competitive explanations of the data, and there is no hierarchy of these models. While this context may be relevant for certain applications, in engineering we often have a well-defined hierarchy of models from cheap, low-fidelity models to expensive, high-fidelity models, and thus BMA methods are not of particular interest in the context of uncertainty quantification in CFD problems. In contrast to BMA methods, for which a model hierarchy does not exist, Multi-Level Monte Carlo (MLMC) methods create and utilize such a hierarchy to facilitate uncertainty propagation by running the same simulator on a series of successively refined meshes, leading to a sequence of multi-

level models. By optimizing the number of simulations conducted on each level, significant speedup compared to the standard MC method has been obtained [4]. However, the MLMC method in essence is a control variate based *variance reduction* technique with two critical assumptions [5]: (1) the ensembles computed on different levels are all *unbiased* estimators of the QoI, and (2) the variance of the estimator decreases as the mesh is refined. These assumptions are also used in the multi-model extension [6]. Therefore, model discrepancies are not accounted for in MLMC methods. In turbulent flows applications, however, model discrepancies play a pivotal role, and thus the MLMC method is less likely to be applicable, since the assumptions above cannot be fully justified. Data assimilation represents another approach of combining multiple sources of information. Recently, Narayan et al. [7] proposed a framework to assimilate multiple models and observations, which expresses the assimilated state as a general linear functional of the models and the data. In general, model discrepancies are not explicitly considered in data assimilation methods, although the available data may implicitly correct any biases in the model predictions in the filtering operations. Similar to MLMC methods, the filtering operations in data assimilations aim to reduce variances of the overall estimation from several unbiased sources.

Gaussian process (GP) is a promising approach to account for model discrepancies. The basic assumption is that the quantities of interest at different design points obey multivariate joint Gaussian distributions. With this assumed correlation, Bayesian updating can be used to infer the distribution of the QoI in the entire field from the data available at certain locations. Results obtained from the Bayesian inference can be viewed as a probabilistic response surface, i.e., mean predictions with quantified uncertainties. Gaussian processes are routinely used to construct the prior in geostatistic and atmospheric inverse problems [8–10]. In engineering design optimization it is used to build surrogate models based on simulations performed at a small number of points in the parameter space [11, 12]. Kennedy and O’Hagan [13] developed the first multi-model prediction framework accounting for model discrepancies by using Gaussian process and Bayesian inference. An important assumption of their framework is that the predictions from different levels are auto-regressive. That is, the higher-level model prediction z^H is related to the lower level model prediction z^L by a regressive coefficient ρ and a discrepancy δ , i.e., $z^H = \rho z^L + \delta$, where δ is described by a GP. Another assumption is that the prior for the prediction of each model can be described by stationary GP. Simulation data obtained from all models are then used to infer the predictions of the highest-fidelity model. More than a decade after being proposed, although this multi-fidelity modeling framework has been used and developed in mechanical and optimizations [12, 14], it has yet to find widespread use for the CFD applications, and thus much more investigations are still needed.

The objective of this work is to account for model discrepancy in the propagation of input uncertainties in CFD applications. Information from models of multiple fidelities is used to enable efficient propagation of input uncertainties. In fluid dynamic problems, the low-fidelity models (e.g., panel methods) are relatively cheap computationally, with each evaluation taking only seconds or minutes. Consequently, the input parameter space can be sampled sufficiently when performing low-fidelity simulations, and thus Gaussian process modeling of the interpolation errors for the low-fidelity predictions as conducted in Kennedy and O’Hagan [13] is largely unnecessary. Therefore, we propose a simpler method based on the framework of [13] and classical Bayesian approach. Specifically, we describe only the

model discrepancy δ between the low- and high-fidelity models (z^L and z^H , respectively) with Gaussian processes without assuming the responses themselves to have a certain distribution. We propagate a large ensemble \mathcal{D}^L by using a low-fidelity model z^L , and then use realizations of model discrepancies (i.e., random draws from the fitted Gaussian process \mathcal{GP}) to correct z^L . With this strategy the distortion caused by low-fidelity model deficiency on the output uncertainty distribution can be reduced with the information provided by the high-fidelity simulations. Previous authors have used GPs and multi-model framework to improve predictions [e.g., 15, 16] and to serve as surrogate models in design optimizations [e.g., 11, 12, 17, 18]. However, to the authors' knowledge, the use of GPs and multi-fidelity models to account for model discrepancies and to perform implicit model calibrations in uncertainty propagation for CFD applications is a novel development. The coupling between model uncertainties and input uncertainties is a unique issue in using GP-based probabilistic response surface for uncertainty propagation, and this challenge is not present when using GP for predictions or optimizations. This issue will be discussed in detail with the complete synthetic cases in the electronic supplementary materials.

The rest of the paper is organized as follows. The methodology and algorithm of the multi-model uncertainty propagation scheme are presented in Section 2. Test cases are investigated to demonstrate the proposed method, and the results are presented in Section 3. The comparison of the multi-model strategy with traditional single-model approaches are discussed in Section 4. Finally, Section 5 concludes the paper.

2. Methodology

An essential part of the proposed uncertainty propagation method is developed based on the multi-model framework of [13]. Specifically, we use the high-fidelity simulations performed on a small ensemble, along with the low-fidelity simulations on the same ensemble, to construct a probabilistic response surface for the model discrepancy δ . Samples drawn from the probabilistic response surface are then used to correct the low-fidelity simulations, which can be performed on an ensemble as large as required. The correction of the low-fidelity results by using data from the high-fidelity simulations can be considered implicit model calibration. In this section, we first introduce Gaussian process modeling and Bayesian inference of model discrepancy in Section 2.1. The overall algorithm of the multi-model uncertainty propagation is then presented in Section 2.2.

2.1. Gaussian Process Modeling and Bayesian Inference of Model Discrepancy

Referring to the airfoil example again, the model discrepancy δ is approximated by the difference between the lift coefficients predicted by the low- and high-fidelity models, and its magnitude depends on the AoA, denoted as input variable x . Since it is prohibitively expensive to perform high-fidelity simulations of the flow over an airfoil for a large number of AoA, the discrepancy δ is effectively an unknown function of x . To facilitate modeling, we assume that (1) the discrepancy $\delta(x_i)$ at any location x_i is a random variable obeying a Gaussian distribution, and (2) the discrepancies $\delta(x_i)$, where $i = 1, \dots, n$, at any number of n locations have a joint Gaussian distribution. Consequently, the unknown function $\delta(x)$ is a Gaussian process, which is expressed as [19]:

$$\delta(x) \sim \mathcal{GP}(m, k), \tag{1}$$

where the mean function $m(x)$ is the expectation of $\delta(x)$; the covariance or kernel function $k(x, x')$ dictates the covariance between the values of function δ at two locations x and x' .

In this work it is assumed that the low-fidelity model is explicitly calibrated beforehand with the best available information (but not against high-fidelity simulation results) to eliminate any bias over the entire input parameter domain, and thus a zero mean function $m(x) = 0$ is used. Note that the zero mean function represents the prior of model discrepancy without information from high-fidelity results and can be corrected by incorporating high-fidelity data through Bayesian updating. We also can assign the prior $m(x)$ with a polynomial function, but it means that more hyperparameters are to be inferred, which requires more data from the expensive high-fidelity CFD simulations. Assuming $\delta(x)$ is a smooth function over most part of the parameter domain, the following kernel function is chosen, i.e.,

$$k(x, x') = \sigma_f^2 \exp\left(\frac{-|x - x'|^2}{2l^2}\right) \quad (2)$$

where $|\cdot|$ denotes Euclidean norm, σ_f determines the overall magnitude of the variance, and l is the length scale. σ_f and l are referred to as hyperparameters. This kernel function is stationary in that the covariance between two points only depends on their distances and not on their specific locations. While this may not be a good assumption in some cases, it can be a reasonable choice when only a small amount of data are available, and it is thus adopted in the present study. More sophisticated, possibly non-stationary, kernel functions are possible [19, 20], but this issue is beyond the scope of this work.

If at certain locations $\mathbf{x}_o = [x_1^o, \dots, x_{n_{obs}}^o]^T$ in the parameter space, the values of the discrepancy are $\mathbf{y}_o = [\delta_1^o, \dots, \delta_{n_{obs}}^o]$, the objective is to predict the values \mathbf{y}_p of the function δ at some other locations $\mathbf{x}_p = [x_1^p, \dots, x_{n_{pred}}^p]^T$. Subscripts o and p indicate observations and predictions, respectively. Observations in this work refer to the process of performing low- and high-fidelity simulations to “observe” the values of the discrepancy function at locations \mathbf{x}_o .

Following Arendt et al. [21], a modular approach is adopted here to determine the hyperparameters and the posterior predictions. Specifically, the hyperparameters are first inferred from observation \mathbf{y}_o via Maximum Likelihood Estimation (MLE) before the predictions \mathbf{y}_p are inferred. The hyperparameter pair σ_f and l that maximizes the likelihood of obtaining observation y_o is chosen. In practice, the logarithm of the likelihood p of \mathbf{y}_o conditioned on hyperparameters, i.e.,

$$\log p(\mathbf{y}_o | \mathbf{x}_o, \sigma_f, l) = -\frac{1}{2} \mathbf{y}_o^T K_o \mathbf{y}_o - \frac{1}{2} \log \det(K_o) - \frac{n_{obs}}{2} \log(2\pi) \quad (3)$$

is maximized, $\det(K_o)$ is the determinant of matrix K_o . The optimization is performed with standard gradient-based procedure [19]. Once chosen, the hyperparameters are considered fixed in subsequent inference of \mathbf{y}_p .

Before the values of \mathbf{y}_o are known, the elements in the stacked vector $[\mathbf{y}_o, \mathbf{y}_p]^T$ have a joint Gaussian distribution according to the definition of GP,

$$\begin{bmatrix} \mathbf{y}_o \\ \mathbf{y}_p \end{bmatrix} \sim \mathcal{N}\left(\begin{bmatrix} \mathbf{0} \\ \mathbf{0} \end{bmatrix}, \begin{bmatrix} K_o & K_{op} \\ K_{op}^T & K_p \end{bmatrix}\right), \quad (4)$$

where \mathcal{N} denotes Gaussian distribution. The mean vector $[\mathbf{0}, \mathbf{0}]^T$ is the value of mean function $m(x)$, chosen to be zero, evaluated at $[\mathbf{x}_o, \mathbf{x}_p]^T$. The covariance matrix K is obtained in a similar way by evaluating the kernel function k , and it is partitioned to sub-matrices K_o , K_p and K_{op} , corresponding to the auto-variances of y_o and y_p , and their cross-covariance, respectively. When \mathbf{y}_o is known, the distribution of \mathbf{y}_p conditional on \mathbf{y}_o is still a joint Gaussian, which can be obtained with standard Bayesian inference procedure as the following [19]:

$$\mathbf{y}_p | \mathbf{y}_o, \sigma_f, l \sim \mathcal{N}(K_{op}^T K_o^{-1} \mathbf{y}_o, K_p - K_{op}^T K_o^{-1} K_{op}), \quad (5)$$

which is the posterior distribution of \mathbf{y}_p . In contrast, Eq. (4) specifies the prior distribution of \mathbf{y}_p . The changes in the mean and the covariance of the posterior distribution reflect the new information provided by the observations \mathbf{y}_o .

2.2. Multi-Model Uncertainty Quantification Method

After detailing the procedure of constructing a probabilistic response surface for the model discrepancy above, which is at the core of current multi-model method, we outline below the overall algorithm of the uncertainty propagation referring to the airfoil example above.

Given the joint uncertainty distribution of input x , e.g., the operation conditions (AoA and Mach number), the objective is to find the uncertainty distribution of the QoI, e.g., the lift coefficient. Assuming, again, that the input uncertainties have been characterized with known probabilities, a traditional MC uncertainty propagation procedure consists of the following three steps:

Sampling: Sample the input uncertainty with a space filling method (e.g., the Latin Hypercube sampling [22]) to obtain an ensemble $\mathcal{D}^L = \{x_j\}_{j=1}^{N^L}$, where $j = 1, \dots, N^L$, and N^L is the number of samples in \mathcal{D}^L .

Propagation: Propagate each sample x_j in \mathcal{D}^L with a model z^L , i.e., $f_j = z^L(x_j)$, leading to an output ensemble $\mathcal{F}^L = \{f_j\}_{j=1}^{N^L}$.

Aggregation: Aggregate the output ensemble \mathcal{F}^L to obtain the output uncertainty distribution of the QoI.

If the responses given by the numerical model z^L differ from the true response, the obtained QoI uncertainty distribution would be distorted. Increasing the fidelity of the model used in the propagation step above would generally reduce the model discrepancy and thus decrease the distortion in the output uncertainty. However, high-fidelity models have high computational costs and would reduce the number of samples that can be afforded, leading to increased sampling errors. With given computational resources, increasing the number of samples and increasing the model fidelity contradict each other by competing for resources.

In view of these difficulties, we perform high-fidelity simulations on a small number N^H of samples in \mathcal{D}^H to obtain an ensemble \mathcal{F}^H . Assuming a GP for the prior of the model discrepancy δ as in Eq. (4), the simulation results in ensemble \mathcal{F}^H are then used to obtain the posterior distribution according to Eq. (5). A number N_c of realizations of the discrepancy function are drawn from the posterior distribution to correct the output ensemble \mathcal{F}^L given by the low-fidelity model, with each realization corresponding a corrected

ensemble. The corrections lead to a set of N_c ensembles, which is denoted as $\{\hat{\mathcal{F}}_k^L\}_{k=1}^{N_c}$. In this case each element in the set is an ensemble \mathcal{F}_k^L , where $k = 1, \dots, N_c$. These ensembles are then aggregated to obtain the output uncertainty for the QoI. As mentioned briefly in the beginning of this section, the multi-model strategy for uncertainty quantification uses data from high-fidelity simulations to construct model discrepancy functions to correct low-fidelity model results. This procedure, which is not present in traditional MC methods with single-model approaches, can be considered implicit model calibration. This calibration differs from traditional calibration procedures in two major aspects: (1) it takes into account the errors of calibration data themselves (i.e., the high-fidelity simulation), and (2) it is probabilistic instead of deterministic, considering the interpolation uncertainties of the model discrepancy based on GP assumptions.

Three sampling procedures are required in the multi-model uncertainty propagation method outlined above. The first one, which is used to obtain design set \mathcal{D}^L , is the same as in traditional MC methods and does not need further discussions. In this work we use Latin hypercube sampling to perform this sampling. Another sampling is required to obtain design set \mathcal{D}^H . Since points in this ensemble are used to construct Gaussian processes, we use a deterministic, uniform sampling on the range of parameter domain to minimize the largest possible distance between an arbitrarily chosen point in the domain and the nearest sampled points. More sophisticated sampling schemes are possible [23], which will be pursued in future studies. Finally, correction step involves sampling a *function* from the posterior GP as described in Eq. (5). In practical implementations, only the values of the function at the parameter locations corresponding to the samples in the ensemble \mathcal{D}^L are needed. Therefore, we only sample N^L random numbers with joint Gaussian distribution $\mathcal{N}(\mathbf{0}, K)$, where K is the blocked kernel matrix in Eq. (5). This is performed with standard procedures [19], i.e., a vector $\tilde{\mathbf{x}}$ consisting of N^L independent and identically distributed (i.i.d) random numbers is generated first, and then a transformation $\mathbf{x} = L\tilde{\mathbf{x}}$ is performed to obtain a random vector with desired covariance K , where $LL^T = K$. Eigenvalue decomposition is used to obtain L from K , whose computational cost scales as $O(N^3)$ with N being the size of the random vector \mathbf{x} . This can be expensive when N is large. However, it is worth pointing out that the sample does not involve numerical model evaluations. Various standard techniques are available to reduce the computational expense of this operation, e.g., by partitioning the parameter space via treed schemes [20].

3. Numerical Simulations

In this section we first evaluate the multi-model approach on synthetic cases that are of relevance to CFD applications. Using synthetic cases enables a comprehensive study on scenarios with a wide range of complexities. A realistic CFD case, the compressible flow over a NACA0012 airfoil, is then used to demonstrate merits of the multi-model approach for uncertainty propagation.

3.1. Synthetic Test Case

When choosing test cases, we have the typical problem of airfoil lift coefficient prediction in mind. In line with the example given above, one is interested in the uncertainty distribution of the lift coefficient C_L when the operation conditions (i.e., input variables

such as AoA α , Reynolds number Re) conform to known distributions. The uncertainty propagation involves performing numerical simulations on a number of samples from the input (e.g., $x = [\alpha, Re]$) space to obtain samples in the output C_L space. The simulations can be conducted by using a cheap, low-fidelity model such as panel method, or an expensive, high-fidelity model, or any models with computational costs and fidelities in between. The $C_L(\alpha, Re)$ response surface for a much studied classical airfoil, NACA-0012, is shown in Fig. 1, which are fitted from experimental data [24]. A notable feature of this response surface is the smooth, monotonic increase of C_L with respect to AoA α in most regions and a sharp decrease at certain AoA, corresponding to stall. The flow physics and regime changes are dominated by the AoA, but note that the Reynolds number provides modulations as it influences the angle at which the stall occurs.

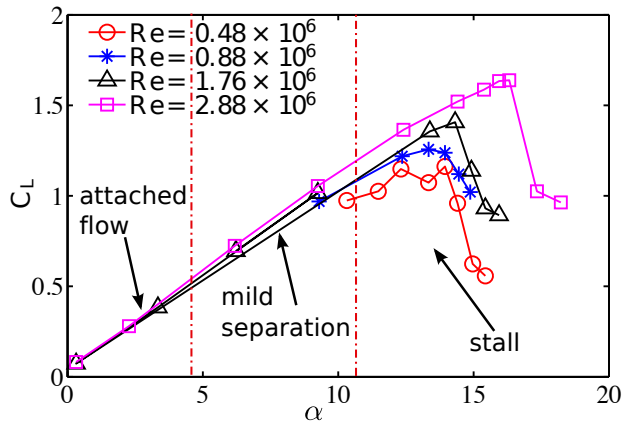


Figure 1: The dependence of the lift coefficient C_L of a NACA-0012 airfoil section on AoA and Reynolds number Re . The three different flow regimes are demarcated with dash-dotted lines.

For the purpose of evaluating the proposed method comprehensively, we first use a few synthetic response surfaces that closely mirror the features of the actual response surfaces in the airfoil example. Specifically, the response surfaces with different complexities from Helton and Davis [22] are used. Due to the space limit, we only present the typical results of the first synthetic response surface in this work. For a comprehensive study on all synthetic cases, please refer to the electronic supplementary materials of this paper. The first response surface has the following expression:

$$f_1(x_1, x_2) = x_1 + x_2 + x_1x_2 + x_1^2 + x_2^2 + x_1 \min(\exp(3x_2), 10). \quad (6)$$

which is a monotonically increasing function with a change of characteristics near plane $x_2 = 0.7$, as plotted in Figs. 2a and 2b. The specific locations of the characteristics change depend on the value x_1 . In this mapping, x_2 dominates the feature of the response surface, and x_1 provides minor modulations, which is reminiscent of the roles of α and Re in the airfoil example. One can compare Fig. 2b with Fig. 1 to appreciate this analogy.

To mimic the behaviors of low-fidelity models (e.g., panel method or RANS solvers) and high-fidelity models (e.g., LES) in CFD applications, the low-fidelity model is constructed by adding a discrepancy function $\delta(x)$ to the true response $f(x)$, with the discrepancy consisting of a constant B and a part that is proportional to f , i.e.,

$$z^L(x) = f(x) + \delta(x) \quad \text{with} \quad \delta(x) = \nu f(x) + B \quad (7)$$

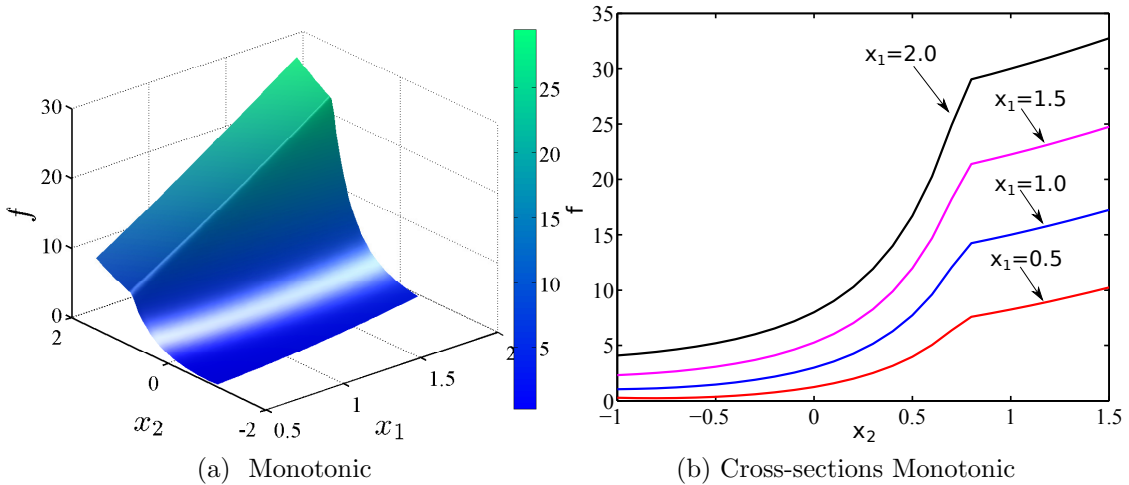


Figure 2: Plots of the synthetic response surface $f(x_1, x_2)$ in Eq. (6). The three-dimensional elevated surface with contour is shown in panel (a), and the cross-sections at several values x_1 are shown in panel (b).

where ν is the proportionality constant, and in all cases, $\nu = 0.2$ and $B = 2$ are used. On the other hand, the high-fidelity model is constructed by adding an i.i.d. noise $\varepsilon(x') \sim \mathcal{N}(0, \sigma_n^2)$ to the true value. The variance σ_n^2 is chosen to be 0.01, which is much smaller than the low-fidelity model discrepancy δ in Eq. (7).

Since the synthetic response has two input variables. To facilitate graphical presentations and to help understand the basic properties of the proposed method, we first test the one-dimensional response surface, which is obtained by fixing the less important variable as $x_1 = 1.25$. The response surface of model discrepancy is constructed with a GP model, and the initial values for hyperparameters σ and l are 1.0 and 0.5, respectively. With five high-fidelity model evaluations, the assumed prior of the model discrepancy is updated by Bayesian approach to obtain the posterior GP. The prior and the posterior are presented in Fig. 3a and 3b, respectively. Figure 3a shows an uninformative prior with relatively large confidence intervals due to the lack of information. Given the “observed” model discrepancy data calculated from the high-fidelity model results at the parameters in ensemble \mathcal{D}^H , the confidence interval of the posterior GP is significantly reduced and the bias error has also been corrected (Fig. 3b). It is noteworthy that the confidence interval is small (but not zero) close to the observation points and increases further away from these points. In most part of the domain, the confidence interval covers the truth, with the exception between $x_2 = -0.5$ and 0.8, where the inferred distribution of δ becomes slightly over-confident. This is due to the fact the modular Bayesian approach, in which the hyperparameters are determined by the MLE method, only accounts for the most likely hyperparameter pair and ignores other less likely possibilities. This inevitably leads to overconfidence, particularly in the cases where the data are sparse, and thus many possibilities are equally likely. With this constructed model discrepancy GP, correction to the ensemble of 500 low-fidelity model results can be conducted by drawing N_c realizations from the posterior GP.

The output ensembles after the correction are aggregated, and their Probability Density Functions (PDF) are plotted in Fig. 4 with comparison to the truth and that obtained with

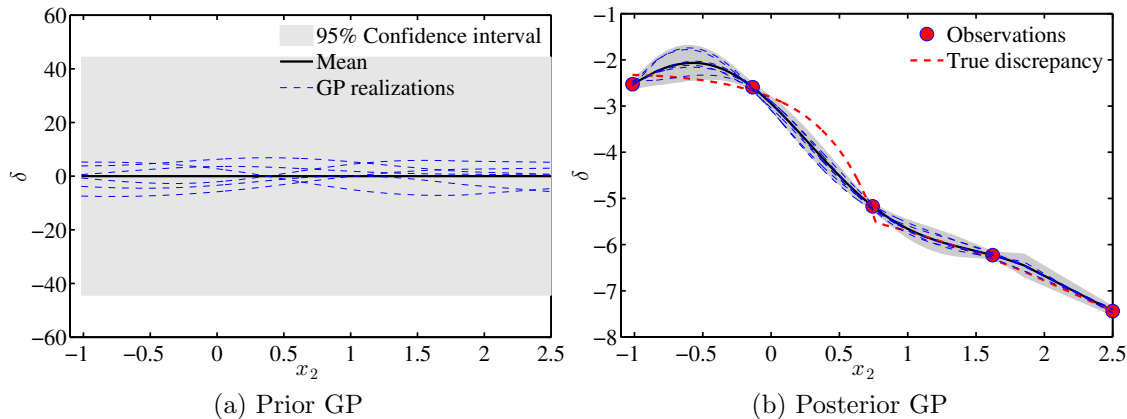


Figure 3: (a) The prior distribution of the model discrepancy function δ is represented as a Gaussian process (GP) with a zero-mean function and a stationary kernel. (b) The posterior GP of δ given observation data at five input locations. In both the prior and the posterior GPs, the mean functions, 95% confidence intervals, and several random realizations from the GPs are indicated.

the low-fidelity model alone. Rigorous, quantitative assessment and comparison of predicted distributions (in the form of PDFs or CDFs) are not straightforward and can be challenging. In this proof-of-concept study we only conduct approximate comparison via visual observations, which can be inadequate when the qualities of two predicted distributions are not obvious. In those cases, more advanced metrics for comparing probability distributions are required, e.g., Area Validation Metric [25] and its modified variant [26]. Figure 4 shows that the normally distributed input uncertainty is mapped to a bi-modal distribution in the output uncertainty distribution. Comparing results in this figure, it is clear that the PDF of the corrected ensemble almost coincides with the corresponding truth, which indicates that the nonlinear model discrepancy has been reconstructed and corrected reasonably well with only five data points from high-fidelity simulations. A minor difference on the left peak and the valley of the PDF is due to the slight overconfidence of the inferred posterior GP as discussed above. This simple case demonstrates that the proposed multi-model scheme can effectively combine the results of models with multiple fidelities to improve uncertainty propagation process. We also evaluate the proposed uncertainty propagation scheme on the synthetic cases with other more complex responses surfaces used in [22], and qualitatively similar improvements are observed (see the electronic supplementary materials).

3.2. Realistic Case in CFD Simulation of Flow Over Airfoil

To illustrate the multi-fidelity uncertainty propagation approach on a realistic CFD case, a turbulent compressible flow over a NACA 0012 airfoil is used as a test example. The input parameters are angle of attack (α) and Mach number (M_∞), and the response is the lift coefficient C_L . In this example the response surface for C_L as a function of α and M_∞ is constructed from solutions of the steady RANS equations. Spalart-Allmaras one-equation turbulence model is employed to calculate the turbulent flow. The airfoil has a chord length of $c = 1$ m, and the simulations are conducted using a density-based solver with an ideal gas equation of state, a free-stream pressure of 101,325 Pa, and a constant molecular viscosity

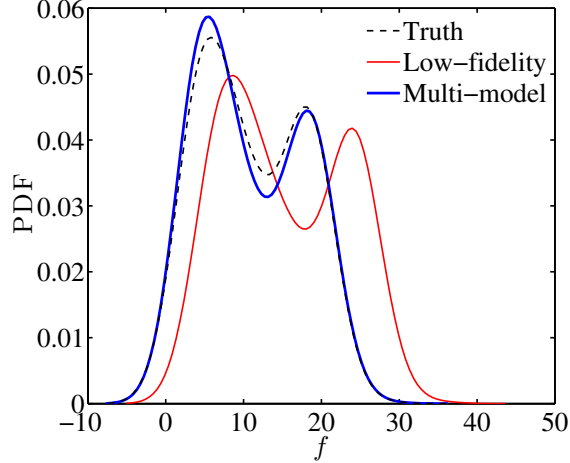


Figure 4: Corrected propagated uncertainty (blue bold solid line) based on the multi-model method compared with original results (red solid line) from the low-fidelity model.

of $\mu = 1.985 \times 10^{-5}$ kg/(ms). Adiabatic, no-slip walls boundary condition is imposed on the airfoil surface, and free-stream far-field is applied to the outer boundary. A matrix of RANS solutions with nine different α and six different M_∞ is used to build the “truth” response surface. This two-dimensional response surface is constructed by the biharmonic spline fits, which ensure the smoothness (see [27] for details). The true response surface for C_l with AoA and Mach number as inputs is shown in Fig. 5a. It can be seen that, similar to the experimental observations, the lift coefficient C_l increases monotonically with respect to AoA in most regions. After certain threshold value of AoA, the lift coefficient C_l decreases markedly, which corresponds to the stall. When the Mach number is small, this sharp decrease of C_l at large AoA can not be observed. The chord-based Reynolds numbers for these Mach numbers are around 1×10^7 .

In contrast to the synthetic case, we use a classic simplified aerodynamics model as the low-fidelity model, where the lift coefficient is calculated based on thin airfoil theory along with the Prandtl–Glauert compressibility correction [28]:

$$C_L^{(L)}(\alpha, M_\infty) = \frac{2\pi\alpha}{\beta} \quad (8)$$

$$\beta = \sqrt{1 - M_\infty^2} \quad (9)$$

Similar to the synthetic case, the high-fidelity model of C_L is constructed by adding an i.i.d. noise to the true value, i.e.,

$$C_L^{(L)}(\alpha, M_\infty) = C_L(\alpha, M_\infty) + \varepsilon, \quad (10)$$

where $\varepsilon(x)$ is a white noise process with variance $\sigma_n^2 = 0.01$. The response surface of the model discrepancy of low-fidelity model $C_L^{(L)}(\alpha, M_\infty)$ is shown in Fig. 5b. As mentioned above, the true mapping $C_L(\alpha, M_\infty)$ is obtained from the RANS simulations, while the low-fidelity model is based on the thin airfoil theory. It can be seen that the predictions from the low-fidelity model are relatively accurate when the AoA and the Mach number are small.

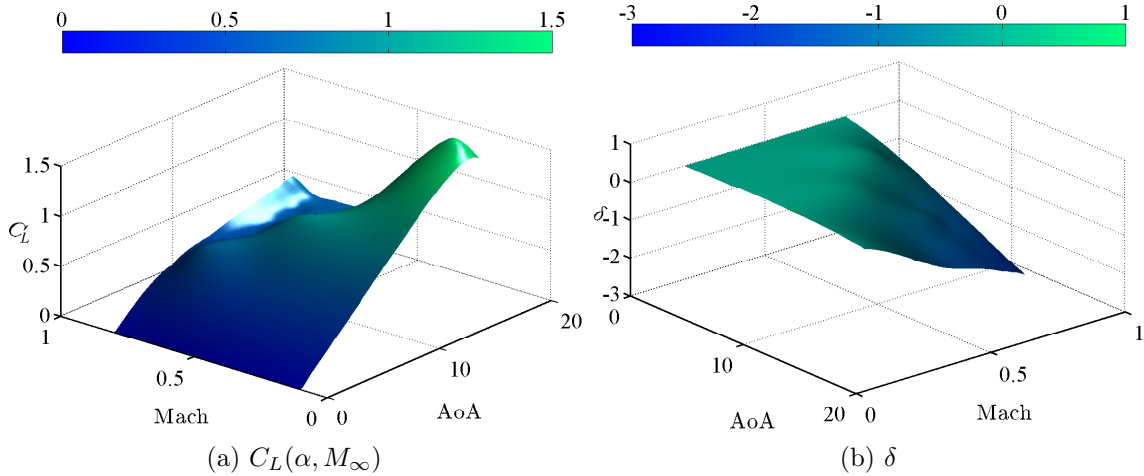


Figure 5: Response surfaces of (a) the mapping $C_L(\alpha, M_\infty)$ constructed by RANS solutions and (b) model discrepancy of low-fidelity model (i.e., thin airfoil theory with the Prandtl–Glauert compressibility correction).

This is because both thin airfoil theory and RANS solver can capture the flow feature and obtain accurate lift predictions in the region of attached flow. However, when the AoA or the Mach number increases, the flow separation occurs, which cannot be captured by the thin airfoil theory. Therefore, large discrepancy can be observed as the AoA or the Mach number is large. Similar to the synthetic case, the response surface of discrepancy here also exhibits monotonic yet nonlinear dependences on the AoA and the Mach number.

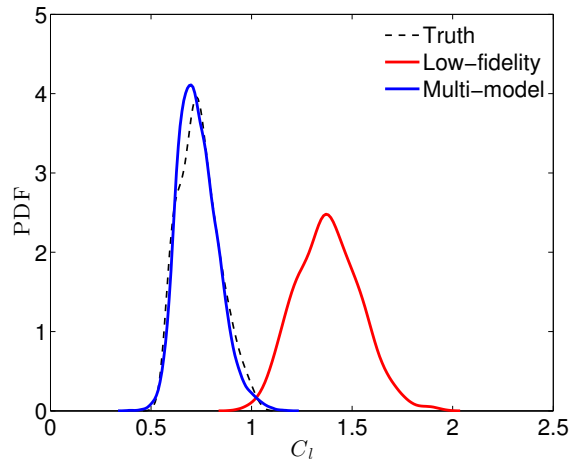


Figure 6: Corrected propagated uncertainty (blue bold solid line) based on the multi-model method compared with original results (red solid line) from the low-fidelity model. Ten high fidelity simulations are used.

In this case, two random input variables α and M_∞ are assumed to be independent and normally distributed with $\alpha \sim \mathcal{N}(10, 1)$ and $M_\infty \sim \mathcal{N}(0.6, 0.06)$, respectively. Similarly, $N^L = 500$ samples are propagated to the QoI, i.e., lift coefficient C_L . The PDF of propagated

samples of C_L is plotted in Fig. 6 with comparisons to the truth and that obtained with the low-fidelity model alone. The normally distributed inputs (α and M_∞) are propagated to C_L (using the multi-fidelity model with 10 high fidelity data), which is also normally distributed with a mean of approximately 0.7. However, the low-fidelity model over-predicts the lift coefficient and its distribution is distorted by the model errors. Similar to the synthetic case, PDF of the corrected ensemble nearly coincides with the corresponding truth, demonstrating the merits of the proposed uncertainty propagation approach.

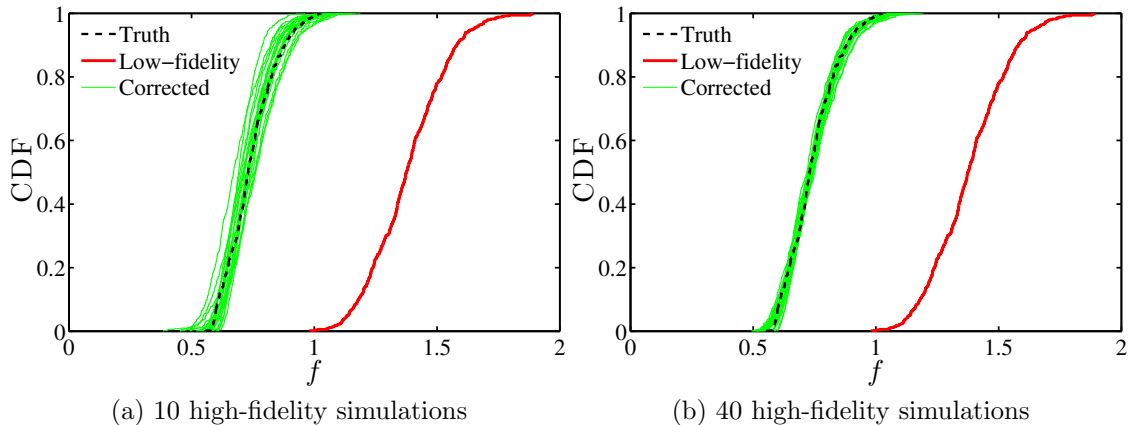


Figure 7: Individual CDFs of QoI corrected by using 30 realizations of the GP (before aggregation) with (a) 10 high-fidelity simulations and (b) 40 high-fidelity simulations.

To investigate the influence of the amount of available data on the propagated uncertainty, we compare the cumulative distribution functions (CDFs) of the C_L ensembles corrected with 10 and 40 high-fidelity data points, where each CDF sample is corrected by an individual GP realization before the aggregation. The CDFs comparison is shown in Fig. 7. For both cases, the probability regions covered by scattered CDF ensembles cover the truth and is significantly improved compared to the low-fidelity results. Note that we use a large number of individual GP realizations to conduct many corrections, instead of using the predicted mean of GP to perform one deterministic correction. Hence, an ensemble of corrected CDFs is obtained instead of a single CDF, which explicitly accounts for the uncertainties introduced by the lack of data. By comparing Fig. 7a and. 7b, we can see that the scattering of CDF samples with 10 high-fidelity data is larger than that with 40 high-fidelity data points. This means the output uncertainty is enlarged, or stated differently, the information entropy increases, when the data is reduced. This is consistent with what we expect that lack of data leads to increase of uncertainty in the propagated distribution, which is referred to as *uncertainty inflation*. In the proposed multi-fidelity strategy, the uncertainties introduced in the reconstruction of discrepancies are obtained based on GP assumptions, and they almost always inflate the propagated input uncertainty. This inflation can be reduced by using more information from high-fidelity simulations.

4. Discussion on Advantage Over Single-Model Approaches

When evaluating the merits of the proposed multi-model approach, there are two legitimate questions to ask before the proposed method can be justified. (1) What benefits does the high-fidelity model offer? Or in other words, would it be better to simply allocate all computational resources to low-fidelity simulations? (2) What benefits does the low-fidelity model offer? Or in other words, would it be better to allocate all computational sources to high-fidelity simulations? Inevitably, answers to these questions are not straightforward, and ultimately they depend on the relative merits and costs of the respective models. Consequently, investigations of these issues can only be based on specific low-fidelity and high-fidelity models. In the following we will discuss the two issues above based on the models assumed in synthetic case.

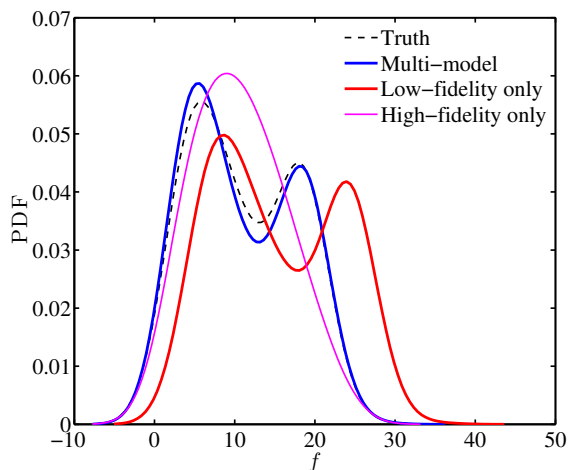


Figure 8: Propagated uncertainty distribution obtained by using the proposed multi-model method compared with those obtained by using the single-model approaches, i.e., with either high-fidelity model or the low-fidelity model alone.

The first question on the benefits of the high-fidelity model has been answered clearly in Section 3 . When the low-fidelity model alone is used in the uncertainty propagation, the obtained output uncertainties show significant biases, which are due to the prediction bias of the low-fidelity models. In contrast, when data from high-fidelity simulations are incorporated into the uncertainty propagation process, even though the amount of available data is very limited, the improvements are clearly visible. This observation effectively demonstrates the value of the high-fidelity model, without which the correct output uncertainty cannot be obtained, no matter how many samples are used in the low-fidelity model evaluations. This is illustrated in Fig. 8, where the PDF obtained by using the low-fidelity model alone shows a significant bias even with a very large ensemble with 500 samples. The second question is closely related to the investigations conducted by Higdon et al. [15] regarding the usefulness of numerical simulations in a prediction method combining numerical simulations and experimental data. They concluded that the numerical simulations have significant contributions in reducing the prediction uncertainties, and thus the combined simulation–data based framework is superior to the pure experimental data-driven approach. Here we carry out a similar

investigation in the context of uncertainty propagation by comparing the multi-model results with those obtained by utilizing high-fidelity simulations alone. That is, in this alternative approach, data obtained from high-fidelity simulations are used to fit a GP, from which samples are drawn to propagate the input uncertainties. The low-fidelity-model is not used in this alternative approach. Results from the simplest one-dimensional response surface from synthetic case discussed in Sec. 3.1, are presented to illustrate the benefits of the low-fidelity model. For this comparison, five high-fidelity model results are adopted for both methods and the same parameters as above are used. The PDF of the QoI uncertainty distribution obtained by using the multi-model approach and that obtained by using the high-fidelity model alone are shown in Fig. 8. From this figure, one can see that the multi-model results agree with the truth extremely well. In contrast, the results from the high-fidelity model alone deviate significantly from the truth. Although the high-fidelity model based approach indeed corrected the obvious bias that is present in the pure low-fidelity model results, it fails to capture the bi-modal feature of output uncertainty distribution, which is an essential feature present in the true QoI distribution. Overall, the multi-model method gives much better results for the QoI uncertainty than the single-model approach based on the high-fidelity model alone. In summary, the comparison above suggests that, by combining the low- and high-fidelity models, the proposed approach produces better results than either model can yield alone.

5. Conclusions

Model uncertainties play an important role in computational fluid dynamics and particularly in turbulent flow applications, where first-principle-based direct simulations are prohibitively expensive and thus are not affordable in most practical applications. In CFD applications, when propagating input uncertainties to QoI uncertainty distributions, uncertainties due to the model used in the uncertainty propagation can distort the obtained output uncertainty. The effects of the model uncertainties on the results should be properly identified, while, at the same time, sufficient samples should be used to avoid sampling errors. In this work we propose a multi-model uncertainty propagation strategy, where model uncertainties are accounted for by using numerical models of different fidelities. Compared to previous work, the proposed method is based on a smaller number of assumptions. In particular, Gaussian processes are not assumed for the low- and high-fidelity models themselves and only for the model discrepancy, which is more realistic for practical CFD applications. Synthetic cases related to CFD applications and a realistic CFD problem are used to demonstrate the merits of the proposed method. Simulation results indicate that biases and distortions of the propagated output uncertainty can be significantly reduced by incorporating data from the high-fidelity simulations through the multi-model framework. Inflation in the propagated output uncertainty associated with the model uncertainty is quantified (see discussion in Sec. 3.2). By incorporating more data from the high-fidelity simulations, the uncertainty inflation can be reduced (see Fig. 7). Overall, the results clearly demonstrate that, by combining the low- and high-fidelity models, the multi-model uncertainty propagation strategy leads to significantly improved results compared with what either model can achieve individually.

References

- [1] O. P. Le Maitre, O. M. Knio, *Spectral Methods for Uncertainty Quantification: with Applications to Computational Fluid Dynamics*, Springer, 2010.
- [2] J. A. Hoeting, D. Madigan, A. E. Raftery, C. T. Volinsky, Bayesian model averaging: a tutorial, *Statistical Science* 14 (4) (1999) 382–401.
- [3] A. E. Raftery, M. Kárný, P. Ettlér, Online prediction under model uncertainty via dynamic model averaging: Application to a cold rolling mill, *Technometrics* 52 (1) (2010) 52–66.
- [4] S. Mishra, C. Schwab, Sparse tensor multi-level Monte Carlo finite volume methods for hyperbolic conservation laws with random initial data, *Mathematics of Computation* 81 (280) (2012) 1979–2018.
- [5] M. B. Giles, Multilevel Monte Carlo path simulation, *Operations Research* 56 (3) (2008) 607–617.
- [6] F. Müller, D. W. Meyer, P. Jenny, Solver-based vs. grid-based multilevel monte carlo for two phase flow and transport in random heterogeneous porous media, *Journal of Computational Physics* 268 (2014) 39–50.
- [7] A. Narayan, Y. Marzouk, D. Xiu, Sequential data assimilation with multiple models, *Journal of Computational Physics* 231 (1) (2012) 6401–6418.
- [8] N. Cressie, *Statistics for Spatial Data*, Wiley-Interscience New York, 1993.
- [9] S. M. Gourdji, K. L. Mueller, K. Schaefer, A. M. Michalak, Global monthly averaged co2 fluxes recovered using a geostatistical inverse modeling approach: 2. results including auxiliary environmental data, *Journal of Geophysical Research: Atmospheres* 113 (D21).
- [10] C. D. Rodgers, *Inverse methods for atmospheric sounding: theory and practice*, Vol. 2, World scientific, 2000.
- [11] A. I. Forrester, A. Sóbester, A. J. Keane, Multi-fidelity optimization via surrogate modelling, *Proceedings of the royal society A: mathematical, physical and engineering science* 463 (2088) (2007) 3251–3269.
- [12] Y. Xiong, W. Chen, K.-L. Tsui, A new variable-fidelity optimization framework based on model fusion and objective-oriented sequential sampling, *Journal of Mechanical Design* 130 (11) (2008) 111401.
- [13] M. C. Kennedy, A. O’Hagan, Predicting the output from a complex computer code when fast approximations are available, *Biometrika* 87 (1) (2000) 1–13.
- [14] C. Park, R. T. Haftka, N. H. Kim, Remarks on multi-fidelity surrogates, *Structural and Multidisciplinary Optimization* (2016) 1–22.

-
- [15] D. Higdon, M. Kennedy, J. C. Cavendish, J. A. Cafo, R. D. Ryne, Combining field data and computer simulations for calibration and prediction, *SIAM Journal on Scientific Computing* 26 (2) (2004) 448–466.
- [16] L. Le Gratiet, Bayesian analysis of hierarchical multifidelity codes, *SIAM/ASA Journal on Uncertainty Quantification* 1 (1) (2013) 244–269.
- [17] D. Huang, T. Allen, W. Notz, R. Miller, Sequential kriging optimization using multiple-fidelity evaluations, *Structural and Multidisciplinary Optimization* 32 (5) (2006) 369–382.
- [18] Q. Zhou, X. Shao, P. Jiang, Z. Gao, C. Wang, L. Shu, An active learning metamodeling approach by sequentially exploiting difference information from variable-fidelity models, *Advanced Engineering Informatics* 30 (3) (2016) 283–297.
- [19] C. K. Williams, C. E. Rasmussen, *Gaussian processes for machine learning*, MIT Press, 2006.
- [20] R. B. Gramacy, H. K. Lee, Bayesian treed gaussian process models with an application to computer modeling, *Journal of the American Statistical Association* 103 (483) (2008) 1119–1130.
- [21] P. D. Arendt, D. W. Apley, W. Chen, Quantification of model uncertainty: Calibration, model discrepancy, and identifiability, *Journal of Mechanical Design* 134 (10) (2012) 100908.
- [22] J. C. Helton, F. J. Davis, Latin hypercube sampling and the propagation of uncertainty in analyses of complex systems, *Reliability Engineering & System Safety* 81 (1) (2003) 23–69.
- [23] J. Sacks, W. J. Welch, T. J. Mitchell, H. P. Wynn, Design and analysis of computer experiments, *Statistical science* (1989) 409–423.
- [24] N. Gregory, C. O’reilly, *Low-Speed aerodynamic characteristics of NACA 0012 aerofoil section, including the effects of upper-surface roughness simulating hoar frost*, HM Stationery Office London, 1973.
- [25] W. L. Oberkampf, C. J. Roy, *Verification and Validation In Scientific Computing*, Cambridge University Press, 2010.
- [26] I. T. Voyles, C. J. Roy, Evaluation of model validation techniques in the presence of aleatory and epistemic input uncertainties, in: *17th AIAA Non-Deterministic Approaches Conference*, ARC, 2015, pp. 1–16. doi:10.2514/6.2015-1374.
- [27] I. Voyles, C. Roy, Evaluation of model validation techniques in the presence of uncertainty, in: *52nd Aerospace Sciences Meeting (SciTech 2014)*, National Harbor, MD, January, 2014, pp. 13–17.
- [28] J. D. Anderson Jr, *Fundamentals of aerodynamics*, Tata McGraw-Hill Education, 1985.